Lu et al. *NPG Asia Materials* (2022)14:73
https://doi.org/10.1038/s41427-022-00424-1

NPG Asia Materials

ARTICLE Open Access

Contactless manipulation of mixed phase fluids in liquid crystal polymer microtubes assisted with light-driven vortex

Yao Lu[1], Lang Qin[1], Quan Liu[1], Zichuan Li[2], Weijia Zhang[3], Chongyu Zhu[1] and Yanlei Yu[1,4]

Abstract

Smart channels that manipulate liquid motion by anisotropic shape changes represent a promising candidate to construct microfluidics for biochemical analysis. However, the existing systems fail to provide a platform for solid exchange mediums to interact with multiple liquid phases, which is a universal technique to effectively extract, enrich, and precisely detect biomarkers. Herein, a combined photo/magnetic control strategy of mixed phase fluids, which integrates the contactless operations of suspending, depositing, and even separating, is reported for the first time based on a trilayer microtube consisting of a flexible supporting layer, photodeformable liquid crystal polymer, and hydrophilic blocking layer. The asymmetric photodeformation of the liquid crystal polymer generates an internal vortex in the microtube to homogenously disperse solid exchange mediums into various aqueous moving droplets and to enable efficient purification and enrichment of the target biomarkers. A newly constructed homemade portable protein analyzer guided by the combined photo/magnetic control strategy features the advantages of a short detection time (20 min), trace sample consumption (5 μL), and a low detection limit (1 μg mL^{-1}).

Introduction

Droplet-based microfluidic systems are a widely used platform for biochemical analysis due to their low sample consumption and potential for high-throughput screening[1–3]. During the procedures of biochemical analysis, one solid exchange medium has to exchange substances with multiple liquid phases, including complex samples, washing buffers, and detection solutions, for the extraction, purification and detection of biomarkers to produce sensitive and reliable signals[4–6]. Multiple external mechanical control units are required to transport, mix, and separate the solid exchange mediums as well as liquid phases[7,8]. For example, each liquid phase relies on a separate syringe pump for its propulsion, and mechanical mixers are further used to create a vortex for the uniform dispersion of the solid phases into the liquid phases to undergo an efficient reaction[9]. However, these essential mechanical units along with complex external circuits hinder the simplification of microfluidic systems, burdening their applications in developing portable devices for point-of-care testing[10].

Recently, researchers have strived to develop in situ microscale control units (pumps, valves, and mixers) by using smart materials, especially deformable ones, which simplify complicated microfluidic systems and advance the development of portable devices[11–17]. Smart materials directly convert external stimuli into mechanical energy to propel liquid, thus reducing the number of mechanical units. In this case, smart materials serve as both fluid channels and microfluidic control units, thus simplifying the complexity of the microfluidics[16,18]. Photodeformable liquid crystal polymers are promising candidates for smart

Correspondence: Chongyu Zhu (cy_zhu@fudan.edu.cn) or Yanlei Yu (ylyu@fudan.edu.cn)
[1]Department of Materials Science & State Key Laboratory of Molecular Engineering of Polymers, Fudan University, 220 Handan Road, Shanghai 200433, P. R. China
[2]Academy for Engineering and Technology, Fudan University, 220 Handan Road, Shanghai 200433, P. R. China
Full list of author information is available at the end of the article
These authors contributed equally: Yao Lu, Lang Qin

materials to manipulate solid/liquid mixed phases via fast, tunable, and multitudinous anisotropic deformation by controlling the variation in mesogen alignment[19–28]. In previous publications, we proposed a conceptually novel strategy to propel diverse liquid phases by asymmetric photodeformation of newly designed linear liquid crystal polymers (LLCPs)[29–32]. LLCPs with excellent processability were easily processed into 3-dimensional tubular actuators and microfluidic chips with photodeformable channels[29–32]. The asymmetric photodeformation of the LLCP channels induced Laplace pressure that propelled a train of discrete droplets with controllable speed and direction. Moreover, Laplace pressure simultaneously generated a vortex inside the moving droplets for dispersion and transportation of the solid particles[29], therefore providing a platform for solid exchange mediums to exchange substances with multiple liquid phases.

Herein, we present an unprecedented combined photo/magnetic control strategy for contactless manipulation of solid/liquid phases in LLCP microtubes assisted with light-driven vortices. The key component is a photo/magnet-controlled trilayer microtube (PTM) composed of a flexible supporting layer, middle photodeformable layer, and inner hydrophilic blocking layer (Fig. 1a, b). The light stimulus and magnetic field facilitate the suspending, depositing, and separating of liquid/solid mixed phases (Fig. 1c), which capitalize on a vortex generated by a nonuniform distribution of the flow velocities in the PTM. The first prototype of a portable protein analyzer (PPA) was constructed based on this strategy to specifically purify, enrich, and analyze various target proteins in complex samples, exhibiting the advantages of a short detection time (20 min), trace sample consumption (5 μL), and low detection limit (1 μg mL^{-1}).

Materials and methods

Materials

Ethylene-vinyl acetate (EVA) copolymer microtubes (FSFR-125H, radius: 0.6 mm, thickness: 0.1 mm, inner-surface coating of EVA hot melt glue) were purchased from Wolida Ltd., Shenzhen, China. The magnetic nanoparticles (MNPs) (ϕ: 100–200 nm, Fe_3O_4 core, Affimag PEO-NH_2) were purchased from BaseLine® Ltd., Tianjin, China. Other substances purchased for the study include D-(+)-biotin (>98%) and bovine serum albumin (BSA) (Adamas, Beijing, China), egg-white avidin (Shanghai Macklin Biochemical, Shanghai, China), streptavidin (Duly Biotech Ltd., Nanjing, China), biotin-4-fluorecence (Keshun Bio-Technique Ltd., Shanghai, China), phosphate buffer saline (PBS) tablets (Solarbio Science & Technology Ltd., Beijing, China), and C-reactive protein (CRP) (1°Ab-CRP and 2°Ab-FITC; Anyan Biology Ltd., Shanghai, China). Enzyme linked immunosorbent assay (ELISA) kits for chicken avidin and rabbit CRP were purchased from Ruixinbio, Quanzhou, China.

Measurements

The ^{1}H NMR spectra of the monomers and the LLCPs were recorded using a DMX-500 NMR spectrometer (Bruker, Billerica, MA, USA) using tetramethylsilane as the internal standard and $CDCl_3$ as the solvent. The molecular weights of the polymers and their polydispersity indices were measured via gel permeation chromatography (LC-10ADvp, Shimadzu, Kyoto, Japan) using tetrahydrofuran as

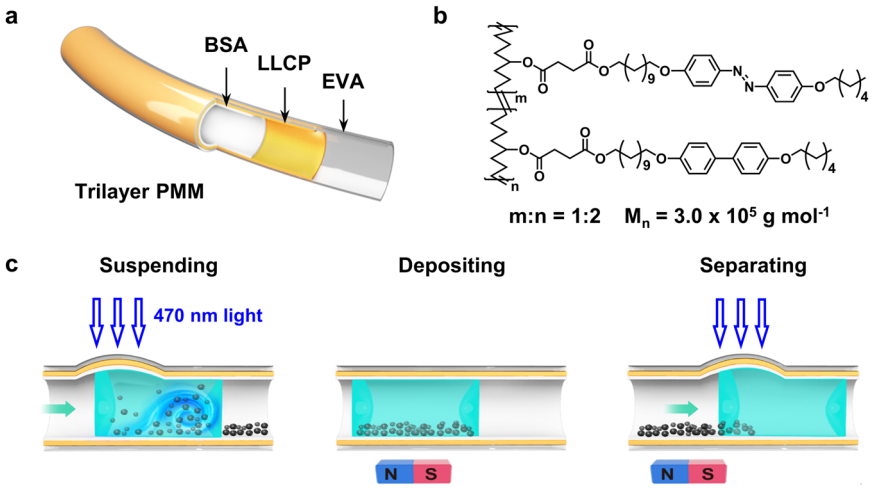

Fig. 1 Design of the combined photo/magnetic control strategy. a Schematic representation of the trilayer photo/magnet-controlled trilayer microtube (PTM) consisting of a flexible supporting layer of the ethylene-vinyl acetate (EVA) copolymer, a photodeformable layer of the linear liquid crystal polymer (LLCP), and a hydrophilic blocking layer of bovine serum albumin (BSA). **b** The chemical structure of the LLCP. M_n is the number-average molecular weight of the LLCP. **c** Schematics showing the detailed operation processes, including suspending, depositing, and separating the liquid/solid mixed phases in the PTM by combined photo/magnetic control. The black particles represent solid exchange mediums.

the mobile phase. The thermodynamic properties of the obtained LLCPs were determined using differential scanning calorimetry (Q2000, TA Instruments, New Castle, DE, USA) at a heating/cooling rate of 10 °C min^{-1} over a temperature range of −10 to 120 °C. A Dataphysics OCA20 system was used to measure the CAs of 3 μL PBS droplets at ambient temperature. To obtain a reliable value, the average CAs were obtained by measuring the same sample in at least five different positions. Adhesion force measurements were performed on a Dataphysics DCAT11. The step rate of the sample plate was set as 0.01 mm s^{-1}, and 3 μL PBS droplets were used. The average adhesion force values were obtained by measuring the same sample in at least five different positions. Photographs of photocontrolled liquid motion were recorded by a camera (Canon 70D). Blue light (λ = 470 nm) was provided by a laser pointer (Chen'en Ltd., Shenzhen, China). An automatic microplate reader (Flex A-200, Allsheng Instruments Ltd., Hangzhou, China) was used to detect the signal of the ELISA kit. A mini-fluorometer (Fluo-100B, λ_{Ex} 460 ± 20 nm, λ_{Em} 525–570 nm, Allsheng Instruments Ltd., Hangzhou, China) was used to detect the fluorescence signal.

Detection of the nonspecific adsorption rate

Droplets of 5 μL avidin solution with a concentration of 0.5 mg mL^{-1} were loaded and incubated in the PTMs before and after BSA modification. The droplets were then exported at intervals to detect the decrease in avidin protein content, which was nonspecifically adsorbed by the PTM inner wall. The avidin content in the supernatant was determined by standard ELISA.

Results and discussion

To manipulate liquid/solid mixed phases in the PTM, we employed a combined photo/magnetic control strategy, used MNPs as a solid exchange medium and used complex sample droplets to demonstrate the detailed processes of suspension, deposition, and separation (Fig. 1c and Supplementary Video 1). When the droplet propelled by light reaches the preloaded band of the MNPs in the PTM, the vortex generated during droplet motion is suspended and disperses the MNPs homogeneously into the droplet. The MNPs deposit rapidly from the droplet with the aid of a magnetic field. The supernatant droplet is removed and separated from the MNPs fixed by the magnetic field.

To use the combined photo/magnetic control strategy, we fabricated a PTM aimed at manipulating solid/liquid mixed phases for protein analysis. The PTM is designed to be (i) flexible; (ii) demonstrate asymmetric deformation; (iii) hydrophilic; and (iv) have ultralow nonspecific adsorption. To attain flexibility, the commercially available EVA copolymer microtube (with outer and inner diameters of 1000 μm and 800 μm, respectively) is chosen as the supporting layer for its good flexibility and comparable modulus. Our designed LLCP with azobenzene and biphenyl side chains in a 1:2 ratio (see Supplementary Fig. 1, 2 and 3 for synthetic routes) is coated on the inner wall of the EVA microtube to achieve asymmetric deformation. As shown in the cross-section photographs of the PTM, the exposed surface of the PTM is displaced by 36.9 μm toward the 470 nm light source (80 mW cm^{-2}) due to the deformation of the LLCP layer, which is attributed to the reorientation of mesogens induced by the Weigert effect (Fig. 2a, b)[33–36]. Such reversible deformation upon intermittent irradiation with 470 nm light can be repeated over 100 cycles without obvious fatigue (Supplementary Fig. 4) because both the high molecular weight and lamellar structure of the LLCP provide sufficient chain entanglement and physical crosslinking[29]. Upon localized irradiation, the regional geometric change of the LLCP/EVA microtube from a cylinder to a conical structure generates Laplace pressure to propel the liquid inside[30]. The PTM is hydrophilic and has ultralow nonspecific adsorption due to modification of the LLCP layer with BSA, a commonly used blocking protein with excellent hydrophilicity in the field of biochemical analysis[36]. Since the reagents used in protein analysis are all aqueous solutions, the BSA layer enhances the hydrophilicity to increase the driving force for propelling the aqueous droplets by Laplace pressure. In addition, BSA plays an important role as a blocking layer to decrease the nonspecific adsorption rate, thus reducing the detection error during protein analysis.

The detailed fabrication processes of the PTM are described in Supplementary Fig. 5. The PTM exhibits the ability to manipulate aqueous droplets of protein analysis reagents by light. As an example, a 5 μL droplet of avidin protein solution retreated from the irradiation site when the PTM was exposed to localized irradiation of 470 nm light (80 mW cm^{-2}) and the droplets direction of movement was reversed by altering the irradiation to the other side (Fig. 2c). Moreover, other kinds of protein analysis reagents, including PBS, MNP suspension, and fluorescence solution, were all manipulated by 470 nm light (80 mW cm^{-2}) in the PTM, traveling at speeds ranging from 0.20 to 0.25 mm s^{-1} (Fig. 2d). The speeds of droplet motion increase gradually with increasing light intensity, and the maximum speed of various protein analysis reagents reaches 0.4 mm s^{-1} (Supplementary Fig. 6).

Figure 2e shows the mechanism of photocontrolled droplet motion in the PTM. The diameter of the exposed wall increases due to the photodeformation of the LLCP layer, while the unexposed part remains unchanged. The Laplace pressure caused by this asymmetric shape change propels the wetting droplets with controllable speed and direction. It should be noted that the photocontrolled motion of aqueous droplets is attributed to the increase in driving force (F_d) and the decrease in resistance (F_r) after BSA

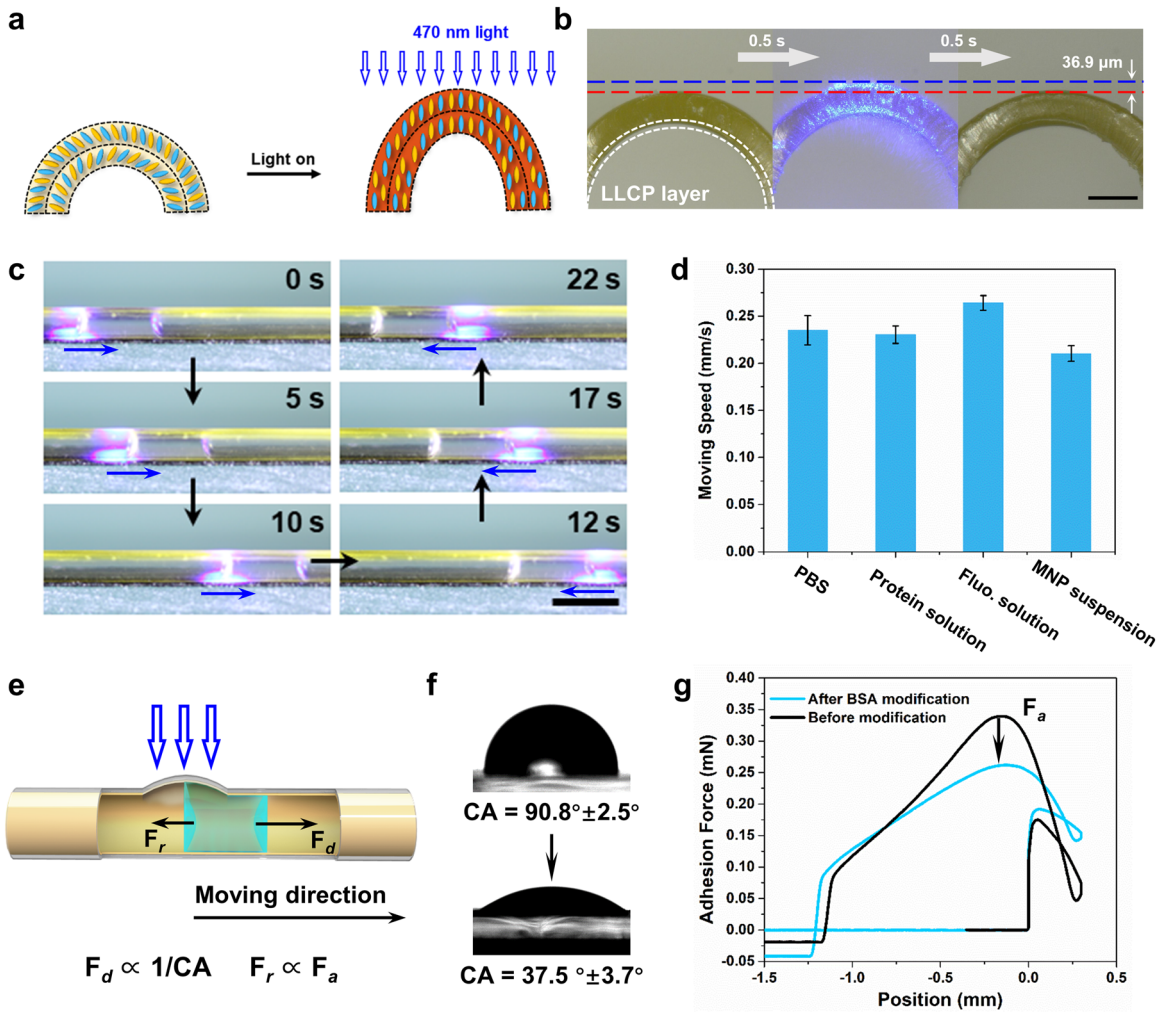

Fig. 2 Characterization of the PTM. a Schematic diagram showing the mechanism of LLCP layer deformation upon irradiation with 470 nm light. **b** Photographs showing local radial expansion of the PTM cross section before and after irradiation with 470 nm light (80 mW cm^{-2}). When the light is switched on, the PTM generates local expansion radially. As a consequence, the exposed surface of the PTM displaces upward 36.9 μm. After continuous illumination for 0.5 s, the displacement of the exposed surface reaches the maximum value. When the light is switched off, the displacement recovers within 0.5 s. The rapid recovery of the PTM is mainly due to the entropic restoring force of exposed regions and the elastic recovery of unexposed regions. Scale bar: 100 μm. **c** Photographs showing the photocontrolled motion of a protein droplet in the PTM. The intensity of the 470 nm light is 80 mW cm^{-2}. Scale bar: 2 mm. **d** Velocities of various reagent solution droplets, including phosphate buffered saline (PBS), protein solution, fluorescence solution, and magnetic nanoparticle (MNP) suspension, used during protein analysis in the PTM. **e** Schematic representation of the force analysis during the photocontrolled motion of droplets in the PTM, where F_d is the driving force, F_r is the resistance force, F_a is the adhesion force, and CA is the contact angle. **f** CAs of a 3 μL PBS droplet on the inner wall of the PTM before (top) and after (bottom) BSA modification. **g** Adhesion force curves of a 3 μL PBS droplet on the inner wall of the PTM before and after BSA modification. The maximum force decreases from 0.339 ± 0.031 mN (black) to 0.259 ± 0.043 mN (blue).

modification. The F_d of the Laplace pressure correlates positively with the wettability of the droplets on the inner wall, and the F_r is related to the adhesion force (F_a) between the droplet and the inner wall. Contact angle (CA) measurements indicate that the CA of a 3 μL PBS droplet on the PTM inner wall decreases from 90.7° ± 2.5° to 37.5° ± 3.7° (Fig. 2f); thus, F_d increases with the enhanced hydrophilicity of the inner layer after BSA modification. The F_a evaluation curve shows that the maximum F_a of the inner layer exerted on 3 μL PBS droplets decreases from 0.339 ± 0.031 mN to 0.259 ± 0.043 mN (Fig. 2g), suggesting the reduction of F_r. According to scanning electron microscope images (Supplementary Fig. 7), BSA on the inner wall forms dendritic crystals, whose microstructures reduce the contact area and, consequently, the F_a between the droplets and the PTM[37]. Therefore, aqueous droplets are propelled in the PTM by combining the asymmetric photodeformation of the LLCP layer and the enhanced hydrophilicity of the BSA layer.

According to the combined photo/magnetic control strategy, a homemade prototype of the PPA was constructed

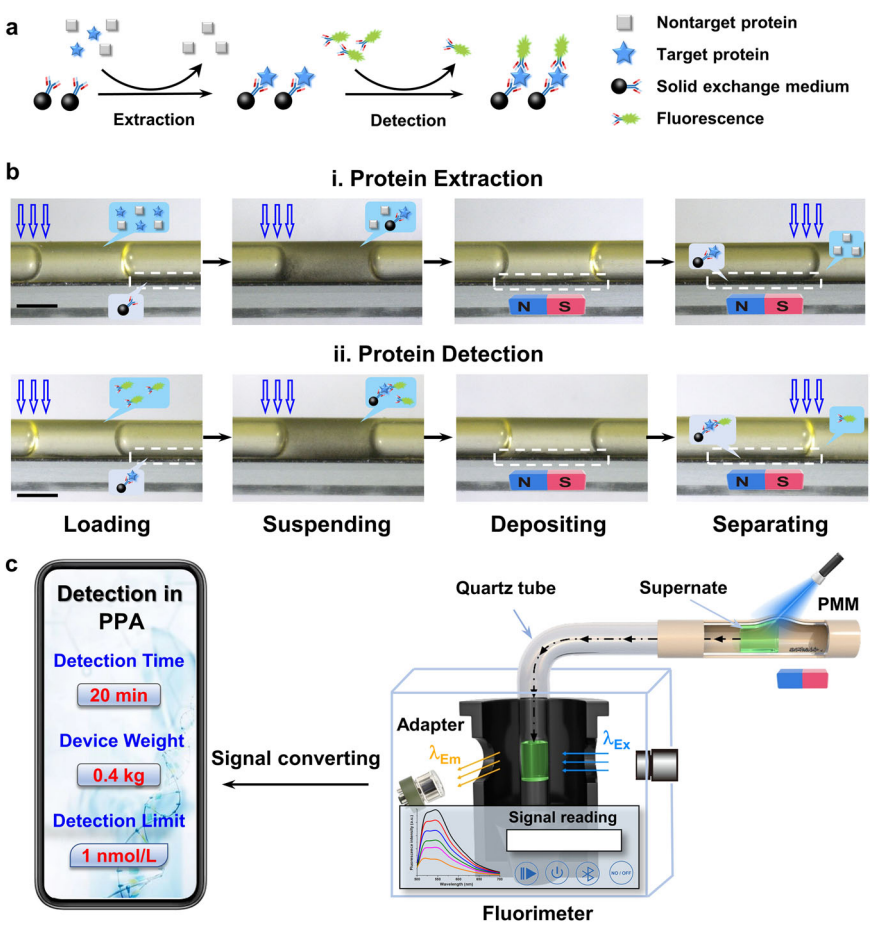

Fig. 3 Operations and construction of the portable protein analyzer (PPA). a Schematics showing the mechanism of protein extraction and fluorescence attenuation detection during protein analysis. **b** Photographs of manipulating solid/liquid mixed phases in the PTM by combined photo/magnetic control, including the processes of loading, suspending, depositing, and separating. (i) Target avidin protein is specifically captured on the biotin-MNPs and extracted from the complex sample. Scale bar: 1 mm. (ii) The biotin-4-fluorescence molecules are bonded to the avidin captured on the biotin-MNPs, which are separated from the supernatant droplet. Scale bar: 1 mm. **c** Schematic representation showing the fluorescence signal measurement of the supernatant droplet, which is exported into the adapter through a quartz tube. λ_{Ex} is the excitation wavelength and λ_{Em} is the emission wavelength. The detected fluorescence signal is recorded by a mini-fluorometer and transferred to a smartphone.

by the PTM, adapter, and mini-fluorometer (Supplementary Fig. 8). MNPs have gained great popularity in microfluidic systems because of their capability to specifically capture various proteins by changing the surface modifiers. Hence, we employed biotin-modified MNPs as a solid exchange medium to demonstrate the extraction and detection of target avidin protein from a complex sample in the PPA by the fluorescence attenuation method (Fig. 3a). The preparation of the biotin-modified MNPs is described in Supplementary Fig. 9, 10 and 11[38]. As shown in Fig. 3b, a 5 μL complex sample is loaded to suspend the biotin-modified MNPs homogeneously, which capture the target avidin protein and then are separated from the supernatant droplet with the aid of combined photo/magnetic control (i. extraction step). In sequence, a 5 μL droplet of biotin-4-fluorescence detection solution, a reported reagent for avidin detection[39,40], is loaded to suspend the biotin-modified MNPs again. The fluorescent molecules are specifically bonded to the target avidin protein captured on the biotin-modified MNPs. After the deposition and separation processes, the supernatant droplet is exported to detect the attenuation degree of the fluorescence signal (ii. detection step). To detect the fluorescence signal of the supernatant droplet, the PTM is connected to an adapter through an L-shaped quartz tube, where the supernatant will be propelled to the detection window from the PTM (Fig. 3c). The adapter is inserted into a mini-fluorometer to measure the fluorescence signal (λ_{Ex} is 460 nm and λ_{Em} is 525 nm). Then, a smartphone is used to convert the fluorescence signal into the concentration information of the target avidin protein in the samples.

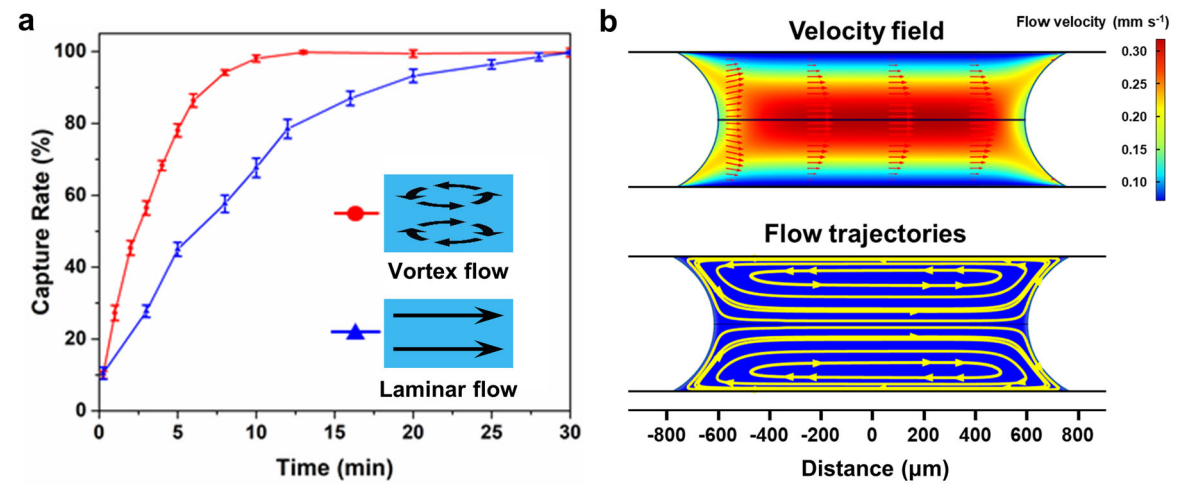

Fig. 4 Finite element analysis in the droplet of the PPA. a A plot showing the capture rate of the target avidin protein as a function of the reaction time in the vortex flow and the laminar flow. **b** Finite element analysis of the velocity field (top) and flow trajectories (bottom) to show the vortex generated in the droplet.

The combined photo/magnetic control strategy provides reliable and time-saving detection results of avidin concentration, the standard curve of which possesses a fitting constant (R^2) up to 0.99998 (Supplementary Fig. 12). The reliable detection results originate from the BSA layer, whose nonspecific adsorption rate is as low as 1.6% (Supplementary Fig. 13)[41]. The capture efficiency of avidin by our strategy is much higher than that observed with conventional microfluidics. As shown in Fig. 4a, 100% avidin is rapidly captured from the complex sample in only 12 min by using the vortex flow, while the time for the same capture rate in the laminar flow is prolonged to 30 min. The high capture rate in the PTM is ascribed to the vortex, which is simulated by the finite element analysis method (Fig. 4b). As shown in the velocity field of the moving droplet, the flow velocity in the center of the droplet is much higher than that at the edge because the edge flow is hindered by the PTM viscous resistance. A nonuniform distribution of the flow velocities leads to the fluid in the center tending to flow to the edge of the droplet, thus forming vortex flow trajectories[42]. The resultant vortex suspended the biotin-MNPs homogeneously and increased the collision probability between the biotin-MNPs and avidin, accelerating the capture procedure.

The droplets in conventional microfluidics driven by syringe pumps exhibited laminar flow, where the solid exchange mediums were difficult to disperse uniformly due to small channel dimensions and uniform flow rates[43]. To generate a vortex, sophisticated channels, including herringbone, zigzag, and serpentine, have been designed to increase channel dimensions and disturb flow rates in conventional microfluidics[44–48]. However, geometric change of the PTM from column to cone spontaneously gives rise to the vortex, resulting from the orientation change of the mesogens upon exposure to 470 nm light. All the operations of liquid/solid mixed phases, including suspending, depositing, and separating, are easily manipulated at the milligram-level with the 3 cm-long PTM by a commercial laser pointer and a magnet.

Table 1 Comparison of the parameters between the commercial microplate reader and the PPA.

	Microplate reader	PPA
Solid exchange mediums	Avidin antibody	Biotin-MNPs
Detection result of egg white (μg mL^{-1})	47 ± 3	51 ± 4
Detection result of cream (μg mL^{-1})	33 ± 2	29 ± 3
Sample consumption (μL)	50	5
Total detecting time (min)	90	20
Equipment weight (kg)	15	0.4
Equipment volume (mm^3)	500 × 300 × 290	194 × 155 × 72.5

The extraction and detection of the target proteins are completed in the PPA in the absence of external mechanical units of the conventional microfluidics[49–53]. We comprehensively investigated the instrument parameters of our homemade PPA and a commercial microplate reader with ELISA kits (see Supporting Information for the detailed steps of protein analysis), which are summarized in Table 1. Egg white and cream were chosen

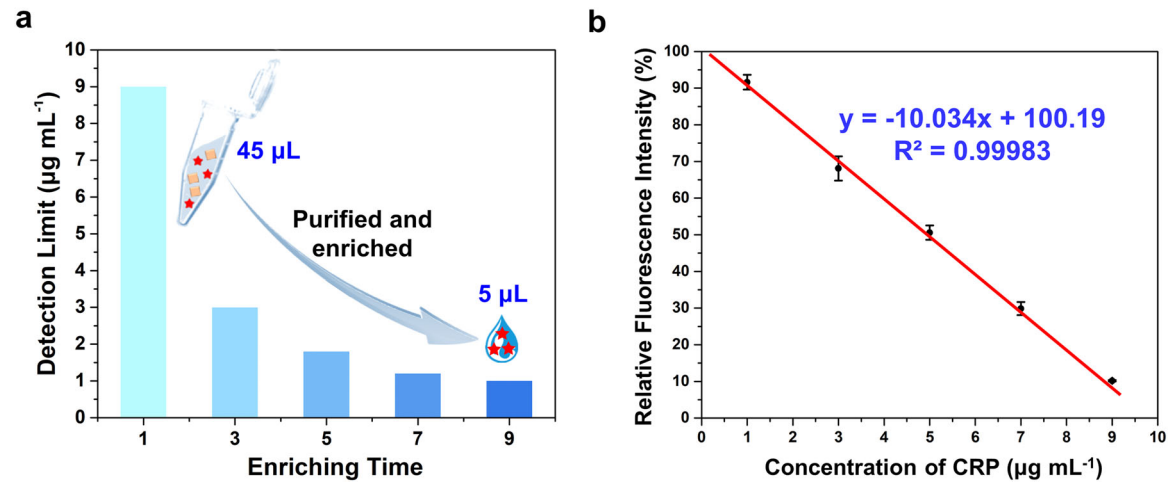

Fig. 5 Protein enrichment by PPA. a A plot showing the minimum C-reactive protein (CRP) detection limit as a function of enrichment time. A 45 μL complex sample was concentrated into a 5 μL droplet after enrichment 9 times. **b** A plot showing the standard detection curve of CRP after enrichment 9 times. The relative fluorescence intensity (y) is inversely proportional to the concentration of CRP (x), and the linear fitting constant (R^2) reaches 0.99983.

as complex samples to analyze the content of avidin by using both the PPA and microplate reader. Compared to the commercial microplate reader, the PPA features comparable detection accuracy and shortens the analysis time from 90 to 20 min. The avidin antibodies fixed on the bottom of the ELISA kit captured the avidin by free diffusion (slow), while the biotin-MNPs were suspended by vortexing in the PPA to accelerate the reaction with avidin (fast). The sample consumption of the PPA is only 5 μL, which is 10 times smaller than that of the microplate reader (50 μL), since the PPA is a droplet-based microfluidic system, where all the processes of protein analysis are performed inside microscale droplets. Moreover, the weight of the PPA is 400 g, approximately 1/40 of that of the microplate reader.

In addition to protein extraction, the homemade PPA has the ability to enrich protein samples with low concentrations, which enables dilute samples beneath the detection limit to be analyzed. For example, CRP, a biomarker of inflammation and cardiovascular disease, has a very low concentration of only 0.8–8 μg mL^{-1} in blood[49]. We demonstrated a decline in the CRP detection limit after enrichment in PPA by using 1°Ab-MNPs as the solid exchange medium and 2°Ab-FITC as the detection solution. The 1°Ab-MNPs captured the CRP from different amounts of 5 μL dilute samples loaded into the PPA sequentially. In this scenario, CRP began to gradually accumulate on the 1°Ab-MNPs after enrichment. The extraction step was repeated several times, and these captured CRP were further specifically bonded to the 2°Ab-FITC in the 5 μL detection solution, whose supernatant droplet was exported to detect the attenuation degree of the fluorescence signal (Supplementary Fig. 14). As a result, the detection limit decreased from 9 to 1 μg mL^{-1} as we increase the number of extraction steps to concentrate the dilute CRP samples from 45 to 5 μL (Fig. 5a). The standard curve with R^2 up to 0.99983 after 9 enrichment steps spans 1–9 μg mL^{-1}, covering the concentration range of CRP in clinical samples (Fig. 5b). Therefore, our homemade PPA provides a versatile platform for fast and accurate protein analysis of various trace complex samples.

Conclusions

In summary, we presented a strategy for contactless manipulation of solid/liquid phases and constructed a PPA prototype with PTMs, detection adapters, and mini-fluorometers for the first time. The trilayer PTM was composed of a flexible supporting EVA layer, middle photodeformable LLCP layer, and inner hydrophilic blocking BSA layer. The LLCP was of significance to generate asymmetric deformation of the PTM, generating Laplace pressure and, importantly, the vortex to propel the droplets and suspend the solid exchange mediums. BSA enhanced the hydrophilicity that increased the driving force to propel the aqueous droplets and played an important role as a blocking layer to decrease the nonspecific adsorption rate and reduce the detection error. The photodeformation and magnetic field were used to manipulate liquid/solid mixed phases for extraction, enrichment, and detection of various proteins, thus replacing complex external mechanical units. It should be emphasized that the light-driven vortex generated during droplet motion dispersed the MNPs into aqueous solutions to effectively capture proteins. Compared to a conventional microplate reader,

the homemade PPA exhibited the advantages of high precision (1 μg mL^{-1}), low consumption (5 μL; 90% reduction), short detection time (within 20 min; 70% reduction), and light weight (only 400 g). Moreover, all the operation processes in the PPA were remotely controlled by light and a magnetic field, avoiding the risk of cross contamination caused by contact manipulation. This strategy opens new opportunities for the integration of photodeformable LCPs into droplet-microfluidic systems, which can facilitate the development of powerful platforms for biomedical diagnosis, food safety applications, and point-of-care testing.

Acknowledgements
This work was financially supported by the National Natural Science Foundation of China (51927805, 51903054, 21734003), the Innovation Program of the Shanghai Municipal Education Commission (2017-01-07-00-07-E00027), and the Natural Science Foundation of Shanghai (19ZR1404500).

Author details
[1]Department of Materials Science & State Key Laboratory of Molecular Engineering of Polymers, Fudan University, 220 Handan Road, Shanghai 200433, P. R. China. [2]Academy for Engineering and Technology, Fudan University, 220 Handan Road, Shanghai 200433, P. R. China. [3]Institutes of Biomedical Sciences & State Key Laboratory of Molecular Engineering of Polymers, Fudan University, 220 Handan Road, Shanghai 200433, P. R. China. [4]Yiwu Research Institute of Fudan University, Chengbei Road, Yiwu City, Zhejiang 322000, P. R. China

Author contributions
Y.Y. and C.Z. conceived the project. Y.L. and Q.L. synthesized the LLCP. Y.L designed and fabricated the PPA prototype. Z.L. analyzed the vortex generation processed by finite element analysis. All the authors analyzed the data. Y.L. and L.Q. wrote the manuscript. Y.L., L.Q., and Y.Y. revised the manuscript. Y.Y. and C.Z. supervised the research.

Competing interests
The authors declare no competing interests.

Supplementary information The online version contains supplementary material available at https://doi.org/10.1038/s41427-022-00424-1.

Received: 8 June 2022 Revised: 27 July 2022 Accepted: 1 August 2022
Published online: 23 September 2022

References

1. Yang, Y., Chen, Y., Tang, H., Zong, N. & Jiang, X. Microfluidics for biomedical analysis. *Small Methods* **4**, 1900451 (2020).
2. Mao, C. et al. Protein detection in blood with single-molecule imaging. *Sci. Adv.* **7**, eabg6522 (2021).
3. Mazutis, L., Baret, J. & Griffiths, A. D. A fast and efficient microfluidic system for highly selective one-to-one droplet fusion. *Lab Chip* **9**, 2665–2672 (2009).
4. Mazutis, L. et al. Multi-step microfluidic droplet processing: kinetic analysis of an in vitro translated enzyme. *Lab Chip* **9**, 2902–2908 (2009).
5. Kecskemeti, A. & Gaspar, A. Particle-based liquid chromatographic separations in microfluidic devices-a review. *Anal. Chim. Acta* **1021**, 1–19 (2018).
6. Zhu, Y. & Fang, Q. Analytical detection techniques for droplet microfluidics-a review. *Anal. Chim. Acta* **787**, 24–35 (2013).
7. Baret, J. Surfactants in droplet-based microfluidics. *Lab Chip* **12**, 422–433 (2012).
8. Bae, J., Lee, J., Zhou, Q. & Kim, T. Micro-/nanofluidics for liquid-mediated patterning of hybrid-scale material structures. *Adv. Mater.* **31**, 1804953 (2018).
9. Matula, K., Rivello, F. & Huck, W. T. S. Single-cell analysis using droplet microfluidics. *Adv. Biosyst.* **4**, 1900188 (2020).
10. Dai, H., Gao, C., Sun, J., Li, C. & Jiang, L. Controllable high-speed electrostatic manipulation of water droplets on a superhydrophobic surface. *Adv. Mater.* **31**, 1905449 (2019).
11. Zhu, C., Lu, Y., Sun, J. & Yu, Y. Dynamic interfacial regulation by photodeformable azobenzene-containing liquid crystal polymer micro/nanostructures. *Langmuir* **36**, 6611–6625 (2020).
12. Wang, Y., Ma, K. & Xin, J. H. Stimuli-responsive bioinspired materials for controllable liquid manipulation: principles, fabrication, and applications. *Adv. Funct. Mater.* **28**, 1705128 (2017).
13. Cheng, Z. et al. Superwetting shape memory microstructure: smart wetting control and practical application. *Adv. Mater.* **33**, 2001718 (2021).
14. Saez, J., Catalan-Carrio, R., Owens, R. M., Basabe-Desmonts, L. & Benito-Lopez, F. Microfluidics and materials for smart water monitoring: a review. *Analytica Chim. Acta* **1186**, 338392 (2021).
15. ter Schiphorst, J., Saez, J., Diomond, D., Benito-Lopez, F. & Schenning, A. P. H. J. Light-responsive polymers for microfluidic applications. *Lab Chip* **18**, 699–709 (2018).
16. ter Schiphorst, J. et al. Photoresponsive passive micromixers based on spiropyran size-tunable hydrogels. *Macromol. Rapid Commun.* **39**, 1700086 (2018).
17. Hou, Y., Xue, Y., Guan, S., Feng, S. & Jiang, L. Temperature-controlled directional spreading of water on a surface with high hysteresis. *NPG Asia Mater.* **5**, e77 (2013).
18. Bare, J. G. et al. Tunable three-dimensional graphene assembly architectures through controlled diffusion of aqueous solution from a micro-droplet. *NPG Asia Mater.* **8**, e329 (2016).
19. Yu, Y., Nakano, M. & Ikeda, T. Directed bending of a polymer film by light. *Nature* **425**, 145 (2003).
20. Finkelmann, H., Nishikawa, E., Pereira, G. G. & Warner, M. A new opto-mechanical effect in solids. *Phys. Rev. Lett.* **87**, 15501 (2001).
21. Li, M., Keller, P., Li, B., Wang, X. & Brunet, M. Light-driven side-on nematic elastomer actuators. *Adv. Mater.* **15**, 569–572 (2003).
22. Wang, M., Lin, B. & Yang, H. A plant tendril mimic soft actuator with photo-tunable bending and chiral twisting motion modes. *Nat. Commun.* **7**, 13981 (2016).
23. Qing, X., Lv, J. & Yu, Y. Photodeformable liquid crystal polymers. *Acta Polym. Sin.* **11**, 1679–1705 (2017).
24. Han, S., Chen, Y., Xu, B., Wei, J. & Yu, Y. An azoester-containing photoresponsive linear liquid crystal polymer with good mesophase stability. *Chin. J. Polym. Sci.* **38**, 806–813 (2020).
25. Gelebart, A. H. et al. Making waves in a photoactive polymer film. *Nature* **546**, 632–636 (2017).
26. White, T. J. & Broer, D. J. Programmable and adaptive mechanics with liquid crystal polymer networks and elastomers. *Nat. Mater.* **14**, 1087–1098 (2015).
27. Gelebart, A. H., Mc Bride, M., Schenning, A. P. H. J., Bowman, C. N. & Broer, D. J. Photoresponsive fiber array: toward mimicking the collective motion of cilia for transport applications. *Adv. Funct. Mater.* **26**, 5322 (2016).
28. Zhu, C., Lu, Y., Jiang, L. & Yu, Y. Liquid crystal soft actuators and robots toward mixed reality. *Adv. Funct. Mater.* **31**, 2009835 (2021).
29. Lv, J. et al. Photocontrol of fluid slugs in liquid crystal polymer microactuators. *Nature* **537**, 179–184 (2016).
30. Xu, B., Zhu, C., Qin, L., Wei, J. & Yu, Y. Light-directed liquid manipulation in flexible bilayer microtubes. *Small* **15**, 1901847 (2019).
31. Liu, Q. et al. An integrated droplet manipulation platform with photodeformable microfluidic channels. *Small Methods* **5**, 2100969 (2021).
32. Liu, Q., Liu, Y., Lv, J., Chen, E. & Yu, Y. Photocontrolled liquid transportation in microtubes by manipulating mesogen orientations in liquid crystal polymers. *Adv. Intell. Syst.* **1**, 1900060 (2019).
33. Yu, Y. & Ikeda, T. Alignment modulation of azobenzene-containing liquid crystal systems by photochemical reactions. *J. Photochem. Photobiol., C.* **5**, 247–265 (2004).
34. Pang, X., Lv, J., Zhu, C., Qin, L. & Yu, Y. Photodeformable azobenzene-containing liquid crystal polymers and soft actuators. *Adv. Mater.* **31**, 1904224 (2019).

35. Qin, L., Liu, X. & Yu, Y. Soft actuators of liquid crystal polymers fueled by light from ultraviolet to near infrared. *Adv. Opt. Mater.* **9**, 2001743 (2021).
36. Jeyachandran, Y. L., Mielczarski, J. A., Mielczarski, E. & Rai, B. Efficiency of blocking of non-specific interaction of different proteins by BSA adsorbed on hydrophobic and hydrophilic surfaces. *J. Colloid Inter. Sci.* **341**, 136–142 (2010).
37. Bhushan, B., Koch, K. & Jung, Y. C. Nanostructures for superhydrophobicity and low adhesion. *Soft Matter* **4**, 1799–1804 (2008).
38. Zhu, Y., Vanga, S. K., Wang, J. & Raghavan, V. Impact of food processing on the structural and allergenic properties of egg white. *Trends Food Sci. Tech.* **78**, 188–196 (2018).
39. Kada, G., Falk, H. & Gruber, H. J. Accurate measurement of avidin and streptavidin in crude biofluids with a new, optimized biotin-fluorescein conjugate. *Biochimica et. Biophysica Acta* **1427**, 33–43 (1998).
40. Kada, G., Kaiser, K., Falk, H. & Gruber, H. J. Rapid estimation of avidin and streptavidin by fluorescence quenching or fluorescence polarization. *Biochimica et. Biophysica Acta* **1427**, 44–48 (1999).
41. Choi, S., Goryll, M., Sin, L. Y. M., Wong, P. K. & Chae, J. Microfluidic-based biosensors toward point-of-care detection of nucleic acids and proteins. *Microfluid. Nanofluid.* **10**, 231–247 (2011).
42. Reyes, D. R., Iossifidis, D., Auroux, P. & Manz, A. Micro total analysis systems. 1. Introduction, theory, and technology. *Anal. Chem.* **74**, 2623–2636 (2002).
43. Shang, X., Huang, X. & Yang, C. Vortex generation and control in a microfluidic chamber with actuations. *Phys. Fluids* **28**, 122001 (2016).
44. Kang, T. G., Singh, M. K., Anderson, P. D. & Meijer, H. E. H. A chaotic serpentine mixer efficient in the creeping flow regime: from design concept to optimization. *Microfluid. Nanofluid.* **7**, 783 (2009).
45. Stroock, A. D. Chaotic mixer for microchannels. *Science* **295**, 647–651 (2002).
46. Oliveira, M. S. N., Pinho, F. T. & Alves, M. A. Divergent streamlines and free vortices in Newtonian fluid flows in microfluidic flow-focusing devices. *J. Fluid Mech.* **711**, 171–191 (2012).
47. Mengeaud, V., Josserand, J. & Girault, H. H. Mixing processes in a zigzag microchannel: finite element simulations and optical study. *Anal. Chem.* **74**, 4279–4286 (2002).
48. Liu, R. et al. Passive mixing in a three-dimensional serpentine microchannel. *J. Microelectromech. Syst.* **9**, 190–197 (2000).
49. Phurimsak, C., Tarn, M. D., Peyman, S. A., Greenman, J. & Pamme, N. On-chip determination of C-reactive protein using magnetic particles in continuous flow. *Anal. Chem.* **86**, 10552–10559 (2014).
50. Xu, H., Liao, C., Zuo, P., Liu, Z. & Ye, B. Magnetic-based microfluidic device for on-chip isolation and detection of tumor-derived exosomes. *Anal. Chem.* **90**, 13451–13458 (2018).
51. Li, J. et al. On-chip, aptamer-based sandwich assay for detection of glycated hemoglobins via magnetic beads. *Biosens. Bioelectron.* **79**, 887–893 (2016).
52. Lafleur, J. P., Jönsson, A., Senkbeil, S. & Kutter, J. P. Recent advances in lab-on-a-chip for biosensing applications. *Biosens. Bioelectron.* **76**, 213–233 (2016).
53. Zhang, P. et al. Ultrasensitive detection of circulating exosomes with a 3D-nanopatterned microfluidic chip. *Nat. Biomed. Eng.* **3**, 438–451 (2019).